The temperature-salinity relationship in the mixed layer

Raffaele Ferrari

1 Introduction

In the surface mixed layer (ML) of the ocean there is a remarkable correlation between the horizontal temperature and salinity gradients. The goals of this project are (1) to investigate if these correlations are the result of processes at work within the ML, (2) to develop parameterizations of these processes to be used in large-scale ocean models.

Observations show abundant examples of horizontal fronts with temperature and salinity that oppose in their joint effect on density on scales of 10 m to 100 km [1], [2], [3]. A useful measure of the degree of compensation is the density ratio R, defined as the ratio of the relative effect of temperature and salinity on a density front. Stommel and Chen ([4], [5]) computed density ratios from large scale meridional temperature-salinity ($T-S$) gradients in the range of latitudes between 20° and 50° and concluded that R has a mean close to 1.7, even though individual fronts can have a density ratio markedly different from 1.7. These results are obtained from climatological data sets and refer to density ratios on scales of thousands of kilometers averaged over a number of years. On smaller horizontal scales, between 20 m and 10 km, Rudnick and Ferrari find that the ML density ratio is 1 and not 2 [3]. These observations imply that the mean density ratio on large scale is 1.7, even though typical thermohaline gradients at small scale have an instantaneous density ratio of 1.

One possible explanation of the correlations between thermohaline gradients in the ML is that atmospheric forcing and entrainment of thermocline waters create and juxtapose water masses with compensating $T-S$ gradients. However the ratio of heat to freshwater buoyancy fluxes is variable in large scale maps and in time series at a point and there is no evidence that these fluxes force a small scale frontal density ratio of 1 and a large annual mean density ratio of 1.7. In this project we propose an alternative interpretation that relies on regulating mechanisms in the ML to create correlations between temperature and salinity, regardless of the large scale atmospheric forcing. Furthermore we show that the processes responsible for these correlations are not properly represented in large-scale ocean models and we suggest more appropriate parameterizations.

2 Nonlinear diffusive parameterizations of eddy transfer of heat and salt in the mixed layer

The basic idea of this study is straightforward: temperature and salinity are dynamically active in ML because they contribute to density gradients. All processes that depend on density gradients, and not on temperature and salinity gradients separately, are potentially

capable of creating $T-S$ relations, because they act only on $T-S$ fluctuations that reinforce in their joint effect on density. In order to test this idea, we first derive parameterizations of the ML, which use density gradients as the driving field, and then we examine the consequences of these parameterizations on the distributions of temperature and salinity in numerical models.

Let us consider the dispersion of some tracer of concentration $\theta(x, y, z, t)$ in the ML. We model the ML as a vigorously mixed shallow layer characterized by a high aspect ratio, i.e. with a depth H much less than the horizontal scale L. The main point here is that there are two very different time scales: a fast time scale over which the layer is mixed vertically and a slow time scale associated with horizontal transports. We argue that in order to describe the lateral dispersion of the tracer on the slow time scale, it is not necessary to resolve the details of the processes active on the fast time scale. The combined action of small scale stirring stirring and vertical mixing can be parameterized as a diffusion of the vertically averaged tracer.

A mathematical model for the horizontal transport of tracers in the ML is formulated decomposing θ in a "mean" – denoted by $\overline{\theta}$ – defined as the average over the depth H of the ML and over a period long compared to the time scale of vertical mixing, and in an "eddy" – denoted by θ' – defined as the departure from that mean. The Reynold's averaged equation for a conserved tracer is

$$\overline{\theta}_t + \overline{\mathbf{u}} \cdot \nabla_H \overline{\theta} = -\nabla \cdot \overline{\mathbf{u}'\theta'} + \overline{F}. \tag{1}$$

Here $\mathbf{u} = (u, v)$ denotes the horizontal velocity of the incompressible Boussinseq fluid. The first term in the RHS of (1) is called the eddy flux divergence. Its net effect is to redistribute the tracer within the body of the fluid. The second term, $\overline{F}$, represents the averaged fluxes of tracer from the surface of the ocean (atmospheric forcing) and through the base of the ML (entrainment of thermocline waters). The challenge of this section is to derive a long-term, large-scale equation for the mean tracer, by expressing the eddy fluxes in (1) in terms of mean quantities.

Eddy fluxes of a conserved tracer can be parameterized with closures based on local mean gradients. The argument goes that a fluid particle carries the value of a conserved, and hence transferable, tracer for some length $\mathbf{l}'$, before it is mixed with its new surroundings. If the particle was initially typical of its surroundings then the eddy flux of tracer θ is given by

$$\overline{\mathbf{u}'\theta'} = -\overline{\mathbf{u}'\mathbf{l}'} \cdot \nabla\overline{\theta}, \tag{2}$$

where it is assumed that $\nabla\overline{\theta}$ varies little over distances comparable with the mixing length $\mathbf{l}'$. The tensor $\overline{\mathbf{u}'\mathbf{l}'}$ defines the eddy diffusivity. The most commonly used parameterization of horizontal eddy transports in the ML is to assume a down-gradient Fickian diffusion,

$$\overline{\mathbf{u}'\theta'} = -k\nabla\overline{\theta}, \tag{3}$$

where k is set to an a priori value constant both in space and time. However down-gradient diffusion follows from (2) only if the statistics of the eddy field are horizontally homogeneous and isotropic. In the ML lateral eddy transports on time scales longer than the vertical mixing time result from hydrodynamical instabilities that release the gravitational potential energy stored in horizontal density gradients. The dynamics is simple; lateral density gradients slump under the action of gravity and drive horizontal eddy fluxes. The eddy velocity $\mathbf{u}'$ and

the eddy displacement $\mathbf{l}'$ associated with the release of potential energy must be, on average, in the direction of the density gradients and larger when the horizontal density gradients are larger. Therefore in the ML the statistics of the eddy field are not homogeneous and isotropic and a down-gradient Fickian closure is not appropriate. It seems natural to look instead for closures that include the effect of large scale density gradients. A general expression for the eddy diffusivity tensor can be written in the form,

$$\overline{\mathbf{u}'\mathbf{l}'} = \gamma f(|\nabla\overline{\rho}|)\nabla\overline{\rho}\nabla\overline{\rho}, \tag{4}$$

where ρ is the density of the fluid, γ a constant and $f(|\nabla\rho|)$ a function whose form depends on the details of the hydrodynamic instabilities that dominate in the eddy field. The corresponding flux of tracer is,

$$\overline{\mathbf{u}'\theta'} = -\gamma f(|\nabla\overline{\rho}|)\left(\nabla\overline{\rho}\cdot\nabla\overline{\theta}\right)\nabla\overline{\rho}. \tag{5}$$

Notice that, even though the flux is in the direction of the mean density gradient, $\overline{\mathbf{u}'\theta'}\cdot\nabla\overline{\theta} < 0$; thus the flux of tracer tends to be down the tracer gradient. With (5) we can write down an equation that describe the dispersion of the mean tracer,

$$\theta_t + \mathbf{u}\cdot\nabla\theta = \gamma\nabla\cdot[f(|\nabla\rho|)(\nabla\rho\cdot\nabla\theta)\nabla\rho] + F, \tag{6}$$

where we dropped the overbars. Hereinafter we assume that all variables are averaged over the depth of the ML and over times longer than the vertical mixing time.

We can now turn to the case where the tracers are temperature T and salinity S. Let us express density as $\rho = \rho_0\left[1 - g^{-1}B\right]$, where B is buoyancy. Assuming that the equation of state is linear, and using suitable definitions, the buoyancy is

$$B = T - S. \tag{7}$$

With our definitions, S, T and B all have the dimensions of acceleration. The nonlinear diffusion equations that describe the buoyancy driven dispersion of heat and salt in the ML follow from (6),

$$T_t + \mathbf{u}\cdot\nabla T = \gamma\nabla\cdot[f(|\nabla B|)(\nabla B\cdot\nabla T)\nabla B] + F_T, \tag{8}$$

$$S_t + \mathbf{u}\cdot\nabla S = \gamma\nabla\cdot[f(|\nabla B|)(\nabla B\cdot\nabla S)\nabla B] + F_S, \tag{9}$$

where F_T and F_S represent the forcings on temperature and salinity.

Parameterizations in which the dynamics depends exclusively on horizontal density gradients are not new to the oceanographic literature. The idea descends from Stommel's two-box idealization of the thermohaline circulation [6]. Stommel posited a transport law in which the exchange of mass between boxes is proportional to the square of the density difference. Some thirty years later Stommel and Young used the same model to study the $T-S$ relation in the ML [7]. Stommel's model is essentially a two-grid points discretization of (8) and (9) with $f(|\nabla B|) = |\nabla B|^{-1}$. Other classes of nonlinear diffusion models have been developed for the full range of space and time scale that are of interest to oceanographers: from the planetary scale of the thermohaline circulation, through the deformation scale dynamics of

baroclinic eddies, down to the ageostrophic circulations in shallow water systems. Here we limit our attention to models for the upper ocean. The redistribution of temperature and salinity in the ML is the result of processes that release the potential energy stored in horizontal stratification; viz. buoyancy driven shear dispersion at scales below the deformation radius and baroclinic instability at larger scales. Our goal is now to emphasize the unity of the physical ideas underlying the two processes and to show that both can be described by the equations in (8) and (9).

2.1 Buoyancy driven shear dispersion

W. R. Young, in the first part of this volume, discussed a class of models to parameterize the transport of heat and salt in a ML idealized as a shallow system with strong vertical mixing. He derived a set of nonlinear diffusion equations for T and S, where the nonlinearity arises because the horizontal transport of heat and salt is by shear dispersion, and the shear flow doing the dispersing is driven by slumping horizontal buoyancy gradients. The main point of his presentation was that the lateral diffusivity in such a ML is proportional to the horizontal buoyancy gradient squared. Young's model is a particular case of (8) and (9), with $f(|\nabla B|) = 1$ and no vertically averaged flow, $\mathbf{u} = (0, 0)$,

$$T_t = \gamma \nabla \cdot [(\nabla B \cdot \nabla T)\nabla B] + F_T, \tag{10}$$

$$S_t = \gamma \nabla \cdot [(\nabla B \cdot \nabla S)\nabla B] + F_S. \tag{11}$$

The constant γ depends on the depth H of the ML and on the details of the processes doing the vertical mixing. If mixing is parameterized as an intermittent process that homogenizes the ML at intervals of time τ, one finds that $\gamma = H^2\tau^3/96$ [8]. Different parameterizations agree on the functional dependence of γ on the depth H and the characteristic time of vertical mixing τ.

It is important to discuss the range of oceanic parameters for which the nonlinear diffusion equations (10) and (11) might apply. Shear dispersion mechanisms can act only at horizontal scales larger than H, say 100 m, and shorter than the deformation radius, typically 10 km in the ML, and at timescales longer than the vertical mixing time, say a day. Motions with smaller lengths and higher frequencies are parameterized as "vertical mixing" (e.g. Langmuir circulations and convective overturning). At larger scales the effects of rotation become important and the dynamics change substantially as shown in the next section. For $H = 100$ m and $\tau = 1$ day one obtains $\gamma = 10^{17}$ m^{2}s^3; we use this as a reference value throughout the report whenever we make quantitative statements about our results.

2.2 Buoyancy fluxes produced by baroclinic instability: Green, Stone and Held

At scales larger then the Rossby radius of deformation eddies produced at baroclinically unstable buoyancy gradients can dominate the transports of heat and salt in the ML. Green used the arguments reviewed at the beginning of this section to show that the transfer properties of baroclinic eddies can be parameterized in terms of their large scale structure [9]. Supposing that the transfer of buoyancy occurs in the growing phase of baroclinic eddies, when energy

is extracted by the eddy from the baroclinic zone of the large scale flow, Green deduced the expected form of the eddy diffusivity in the limit of large Richardson number. He then used linear stability analysis of the baroclinic wave to determine the direction of the eddy fluxes. Stone derived a similar expression from linear stability analysis and extended Green's results to small Richardson numbers [10]. Green and Stone imagined that diabatic processes, like vertical mixing, restore the baroclinic zone, replenishing the supply of available potential energy until it is discharged again by baroclinic instability. This repeated conversion of energy leads to a diapycnal eddy flux. Green and Stone attempted to relate this flux to large-scale parameters in zonally averaged models of the atmosphere,

$$\overline{v'\theta'} = -\frac{\alpha}{N} l^2 \, |B_y| \theta_y, \tag{12}$$

where v' is the meridional eddy velocity, N is the Brunt-Väisälä frequency, α a universal constant of proportionality, and l a measure of the meridional eddy displacement. Green argues that this distance is set by the width of the baroclinic zone. Stone, however, suggest that the deformation radius is the appropriate length scale. The ideas of Green and Stone, however, converge on predicting that the baroclinic eddy fluxes across a buoyancy gradient are driven by the absolute value of the diapycnal buoyancy gradient. It then makes good physical sense to extend (12) to two dimensions as,

$$\overline{\mathbf{u}'\theta'} = -\frac{\alpha}{N} l^2 \, |\nabla B|^{-1} \, (\nabla\theta \cdot \nabla B) \, \nabla B. \tag{13}$$

With this parameterization of lateral eddy transports, the dispersion of temperature and salinity in the ML is once again described by nonlinear diffusion equations of the form in (8) and (9); in this case $f(|\nabla B|) = |\nabla B|^{-1}$ and $\gamma = \alpha l^2 N^{-1}$.

Pavan and Held used the results of numerical simulations to test diffusive parameterizations of the buoyancy fluxes produced by baroclinic instability [11]. They integrated a two layer model of a baroclinically unstable jet to obtain a series of statistically steady states for different jet widths and evaluate diffusive approximations of the eddy buoyancy fluxes. In their simulations the flow is forced by relaxation to an unstable prescribed buoyancy gradient. Pavan and Held found that a flux-gradient relationship, deduced by a simple fit on numerical results, predicts the magnitude and the shape of the eddy fluxes in the unstable jet flows remarkably well. The functional form of the relationship differs from that suggested by Green and Stone; for large buoyancy gradients, that is for temperature gradients larger than the climatological mean of 6° C over 1000 km, the effective diffusivity is proportional to the fourth power of the buoyancy gradient. In the presence of two stratifying components, like heat and salt, one obtains a set of coupled equations for temperature and salinity of the form in (8) and (9) with $f(|\nabla B|) = |\nabla B|$.

The main conclusion of this brief review is that different diffusive parameterizations of tracer fluxes produced by baroclinic instability agree on one point: diapycnal baroclinic fluxes can be described with nonlinear diffusive closures where the diffusivity is proportional to some power of the buoyancy gradient. Differences emerge only in the power law that relates the buoyancy flux to its gradient, but all parameterizations are captured by the general form in (8) and (9). The parameterizations discussed so far describe the eddy transports across and not along isopycnal surfaces. A full parameterization of baroclinic instability should account

for the epipycnal fluxes as well. However our goal is to explain how a density ratio of one is maintained in the ML at small scales, even though the ratio of heat and freshwater fluxes is extremely variable in the external forcing. Isopycnal eddy fluxes do not release the energy stored in horizontal buoyancy gradients and thus cannot explain compensation. Therefore we do not attempt a parameterization of epipycnal fluxes in this project, but it remains an open question to verify the role of these fluxes in creating correlations between two dimensional distributions of temperature and salinity.

3 Temperature-salinity correlations at small scales as a result of nonlinear diffusive parameterizations

We begin by exploring the implications of the nonlinear diffusive parameterization of the ML in an idealized setting. Suppose that temperature and salinity variations are created at some instant by atmospheric forcing or entrainment of thermocline waters and that these horizontal nonuniformities disappear as a result of nonlinear diffusion. This is a rundown problem in which there is no external forcing and the down-gradient diffusion eventually erases all the initial fluctuations in temperature and salinity. There is no mechanism to produce new randomness: all the randomness comes from the initial condition. Equations (8) and (9) reduce to

$$T_t = \gamma \nabla \cdot [f(|\nabla B|)(\nabla B \cdot \nabla T)\nabla B]\,, \qquad S_t = \gamma \nabla \cdot [f(|\nabla B|)(\nabla B \cdot \nabla S)\nabla B]\,. \tag{14}$$

Observe that the free decay of temperature and salinity is perfectly symmetric in this system. If the statistics of temperature and salinity are identical in the initial conditions, then no asymmetries in the thermohaline fields can develop at later times. One might then expect that this rundown problem shows only the progressive decay of the initial temperature and salinity fluctuations. However apart from the trivial decay, well before all fluctuations are erased, nonlinear diffusion creates nontrivial correlations between the thermohaline fields and between their gradients. The physical reason is that in the initial conditions there will be regions in which the temperature and salinity gradients will happen to partially compensate in their joint effect on buoyancy. In those regions the nonlinear diffusion will be small and the initially compensating gradients will persist. Likewise, the initial conditions will also contain regions in which the thermohaline gradients accidentally produce large buoyancy changes; those regions are then subject to strong diffusion and the gradients will quickly disappear. The consequence of this selective decay is that only compensated thermohaline gradients persist as the system runs down and a density ratio of 1 is established.

3.1 One-dimensional model

We start by considering the simplest problem in which the temperature and salinity have spatial variations in only the y-direction. Equations (14) then reduce to

$$T_t = \gamma \left(|B_y|^n T_y\right)_y\,, \qquad S_t = \gamma \left(|B_y|^n S_y\right)_y\,, \tag{15}$$

where n is an integer that can take any value from 1 to 3 according to the nonlinear closure under consideration.

The one-dimensional case is sufficient to illustrate the development of thermohaline correlations from random initial conditions. Numerical simulations of the system in (15) are carried in non dimensional variables. Buoyancy, temperature and salinity are measured in terms of the initial RMS buoyancy variations ($\mathcal{B}_0$), lengths in terms of the initial correlation length (ℓ_0), and time in terms of $\tau_\gamma \equiv \ell_0^4/\gamma\mathcal{B}_0^2$. τ_γ is the time it takes to mix tracers over a distance ℓ_0 using nonlinear diffusion driven by the initial RMS buoyancy gradients. In terms of non dimensional variables one simply sets $\gamma = 1$ in (15). The initial conditions are established by selecting T and S uncorrelated at each grid point using a uniform probability density function with zero mean such that

$$\langle B^2 \rangle = 1, \qquad \langle T^2 \rangle = \langle S^2 \rangle = \frac{1}{2}, \tag{16}$$

where $\langle\rangle$ is an integral over the domain

$$\langle B^2 \rangle \equiv \frac{1}{L}\int_0^L B^2 \, \mathrm{d}y. \tag{17}$$

The numerical calculations are performed by integrating the non dimensional coupled equations for temperature and salinity. Global conservation of heat and salt is satisfied by requiring that the gradients T_y and S_y vanish at both ends of the domain (i.e., 'no-flux' boundary conditions). We solve the system in (15) on a discrete spatial grid with an explicit Euler forward scheme in time and central differencing in space. The time step, Δt, is short enough to accurately solve the set of ordinary differential equations obtained by the spatial discretization of (15).

The creation of positive correlations between temperature and salinity and their gradients is shown in a series of $T - S$ and $T_y - S_y$ scatterplots. Figures 1, 2 and 3 show the results of simulations with different nonlinear power diffusivities, respectively $n = 1$, $n = 2$ and $n = 3$ in (15). In all three cases the thermohaline compensation is evident as an extension of the cloud of points along the "compensation line" $T_y = S_y$ at time $t = 3$. A cloud of points collapsed along the "compensation line" is equivalent to a density ratio of 1; thus diffusive parameterizations with a diffusivity that depends on the horizontal buoyancy gradient correctly predict the observed density ratio of 1 at small scales. The reader interested in a more rigorous analysis of these simulations is referred to [8], where the nonlinear diffusion equation with diffusivity $n = 2$ is analyzed both numerically and analytically. Here we want to stress the fact that compensation is typical of all parameterizations that have a diffusivity that grows proportionally with the horizontal gradients of buoyancy. Changing the power law in the diffusive parameterization affects the aspect ratio of the cloud of points in the scatterplots, but not the orientation of the major axis.

Finally let us discuss the characteristic time over which compensation occurs. After the passage of a hurricane, typical temperature gradients can be as large as 0.1 °C over a kilometer. The shear dispersion model for a mixed layer 100 m deep and a vertical mixing time of the order of one day, shows compensation over scales of a kilometer after only one hour. Choosing a vertical mixing time scale of a third of a day gives that compensation is created in one day. More importantly compensation on scales of 10 km is established in a time 100 times slower. Therefore we expect compensation to be restored after each forcing

event on scales of a kilometer, while on larger scales compensation and external forcing act on comparable time scales. This explains why a density ratio of 1 is observed only up to scales of at most 10 kilometers.

3.2 Two-dimensional model

In the previous section we investigated nonlinear diffusive parameterizations in one dimension. We now extend our analysis to two dimensional models. A second spatial dimension adds new flavor to the problem, because the nonlinear diffusion depends not only on the magnitude but also on the relative orientation of the thermohaline gradients.

Numerical simulations of the nonlinear diffusion equation in (14) are carried in dimensionless variables as discussed in the previous section. Conservation of heat and salt is satisfied by imposing periodic boundary conditions at the edges of a square domain. The initial conditions have random and uncorrelated T and S profiles. The numerical integrator uses a third order Adams-Bashford scheme in time and central differences in space. The time step is chosen short enough to ensure stability and accuracy of the solutions.

The two dimensional rundown problem shows that correlations develop between the magnitudes of the thermohaline fields in much the same way described for the one dimensional case. Scatterplots of the thermohaline gradients, computed along an arbitrary path within the domain, collapse along the compensation line during the first phases of the simulation and look exactly like those in figures 1, 2 and 3. The new result is that correlations develop also between the orientation of the thermohaline gradients. Figure 4 shows histograms of the angles between the temperature and salinity gradients at each grid point. The process of "thermohaline alignment" is extremely fast and by time $t = 1$ (of the order of one day or less in dimensional units for typical ML gradients) T and S gradients are nearly everywhere parallel. Note that the number of aligned gradients increases with time, proving that nonlinear diffusion actively tilts the T and S isolines so as to create a uniform buoyancy field. In one dimension compensation is the result of dissipation of all buoyancy gradients. In two dimensions nonlinear diffusion can also create compensated gradients not present in the initial conditions, by selectively dissipating those components of thermohaline gradients that project on density gradients. The results shown in figure 4 are obtained for a shear dispersion closure, that is by substituting $f(|\nabla B|) = 1$ in (14). Analogous results are obtained for the other forms of $f(|\nabla B|)$ introduced in section 2.

The main result of the two dimensional simulations is that nonlinear diffusive parameterizations of the ML produce compensation between the gradients of temperature and salinity along any direction. This is consistent with the density of ratio of 1 measured by profiling the ML along one dimensional paths [3]. It remains to understand why compensation and a density ratio of 1 are observed only at small scales and not at scales of thousands of kilometers. We address this point in the next section.

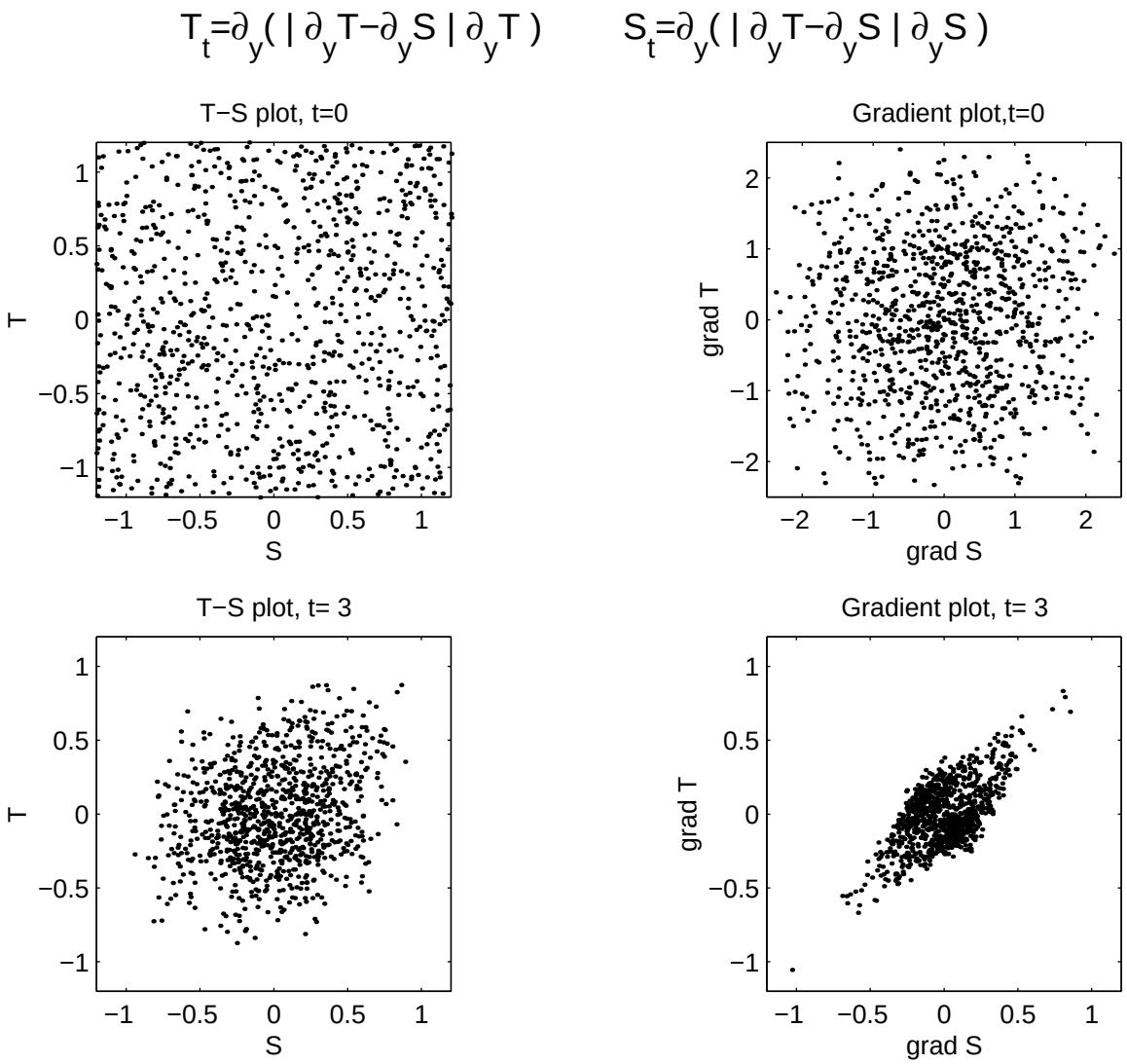

Figure 1: This figure shows the results of a simulation in which 1000 points in the (S, T) and (S_y, T_y) planes are created by picking uncorrelated temperature and salinity from a uniform probability density with variance $1/2$; thus the variance of $B = T - S$ is one. The nonlinear diffusivity is of the form $|B_y| = |T_y - S_y|$. The upper panels show scatterplots at time $t = 0$. The lower panels scatterplots at $t = 3$.

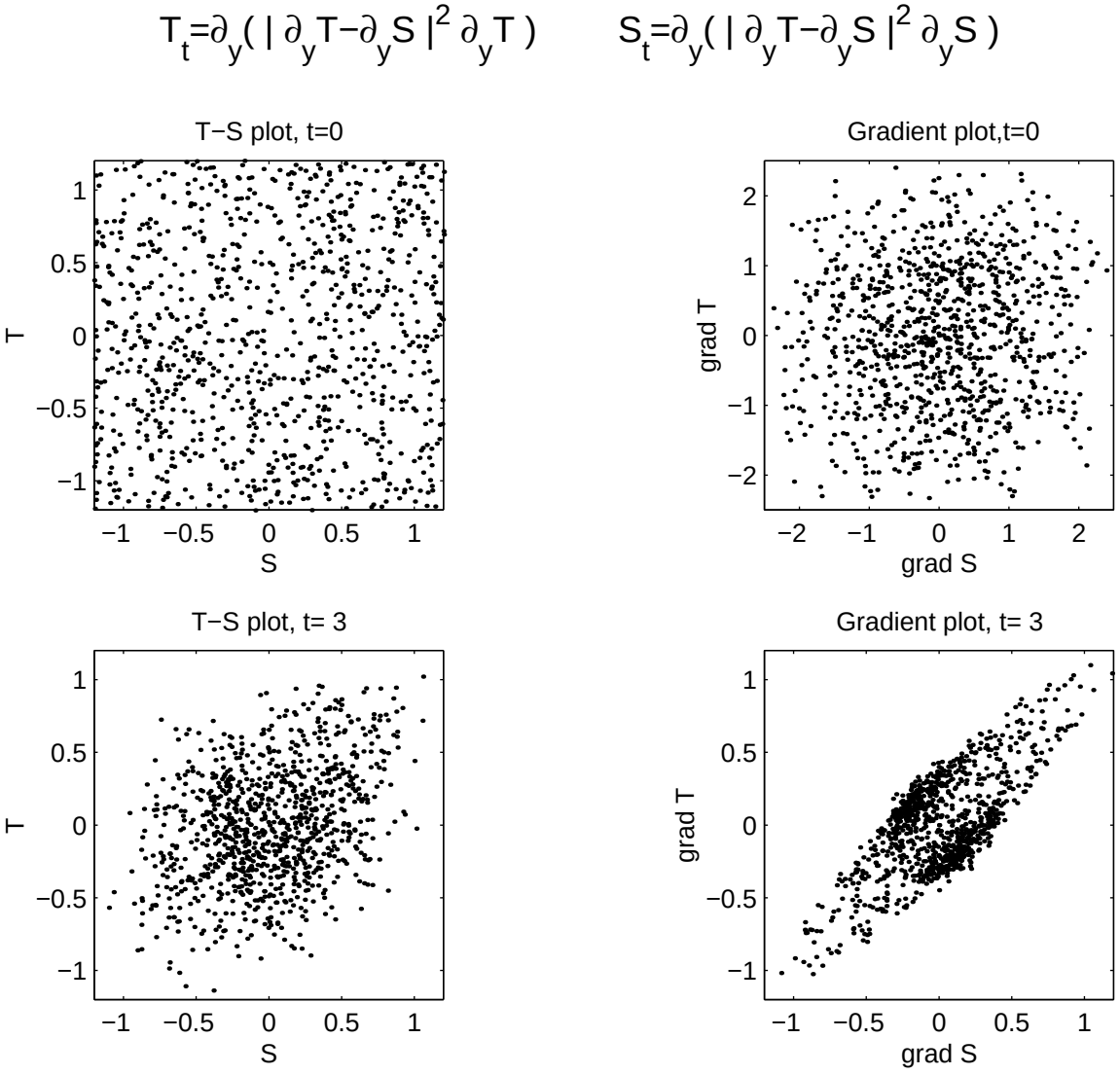

Figure 2: As in figure (1), but with a nonlinear diffusivity of the form $|B_y|^2 = |T_y - S_y|^2$.

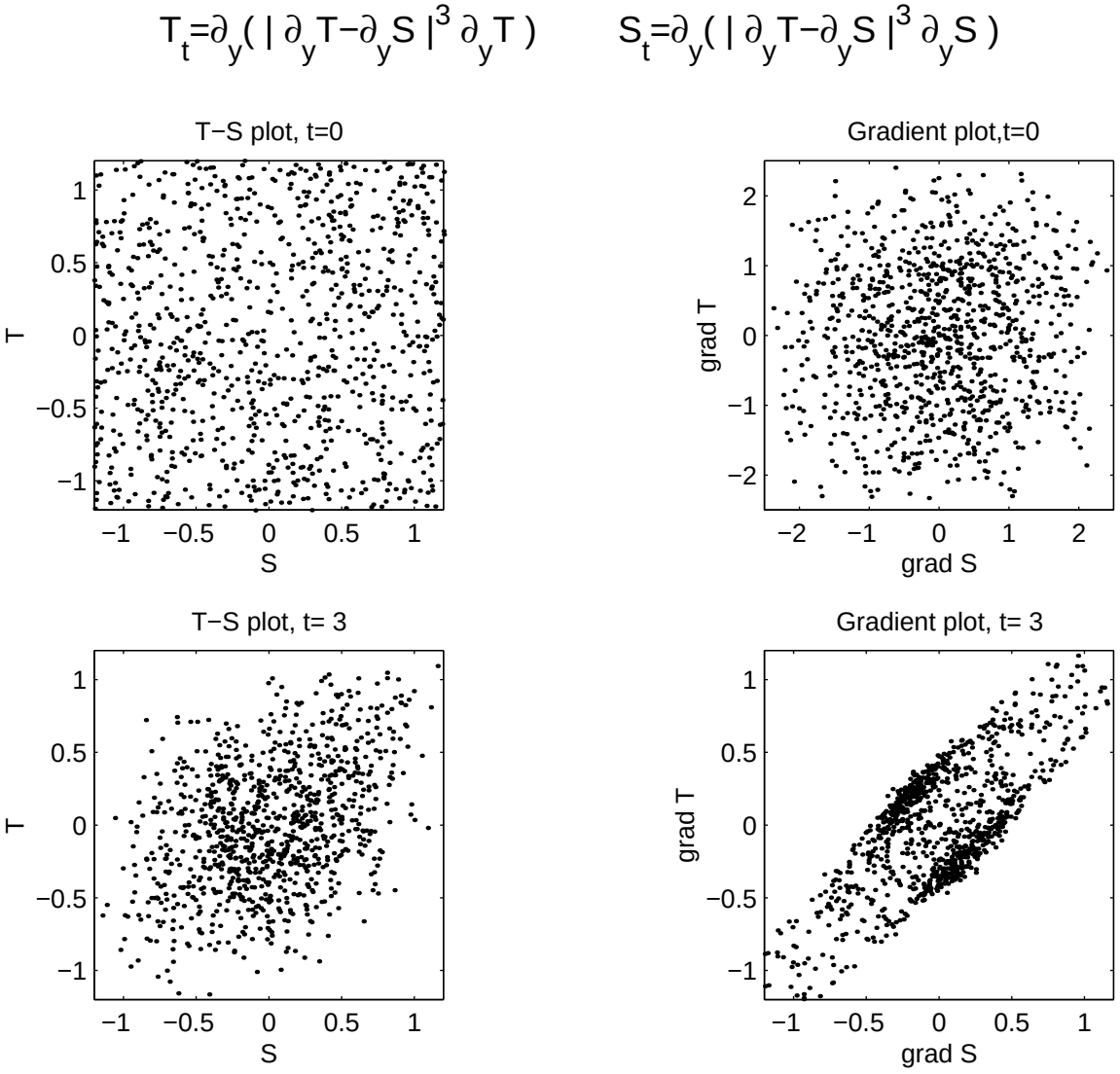

Figure 3: As in figure (3), but with a nonlinear diffusivity of the form $|B_y|^3 = |T_y - S_y|^3$.

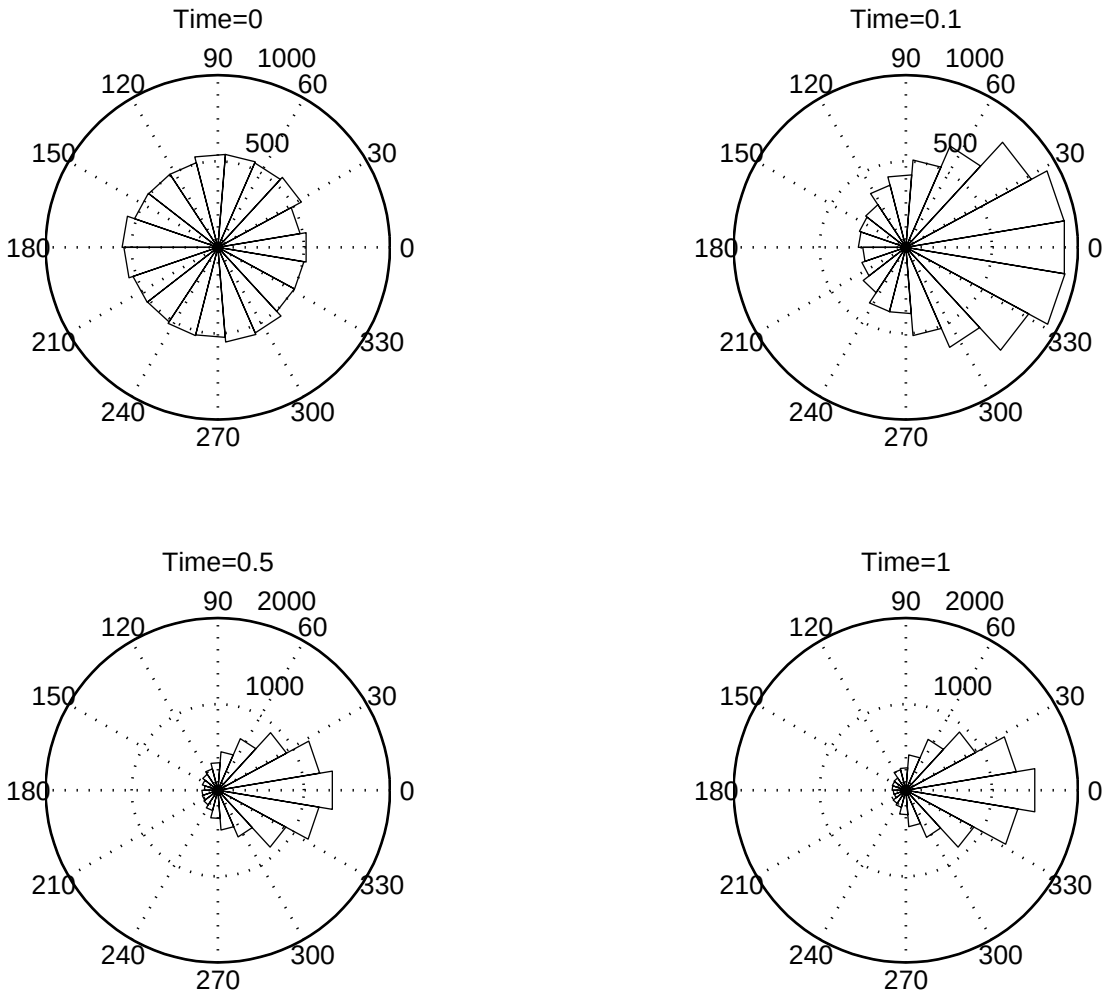

Figure 4: Histograms of the angles between the temperature and the salinity gradients at four different times in a simulations on a grid of 100×100 points. The initial conditions are created by picking uncorrelated temperature and salinity from a uniform probability density with variance $1/2$; thus the variance of $B = T - S$ is one. The thermohaline fields evolve according to the equations in (14) with $\gamma = 1$ and $f(|\nabla B|) = 1$.

4 Temperature-salinity relation at large scales explained with a forced nonlinear diffusion equation

We showed how correlations develop between the thermohaline fields as a result of nonlinear diffusive parameterizations by solving initial value problems in which temperature and salinity are prepared as random and uncorrelated distributions. For typical ML thermohaline gradients these correlations are established on time scales of days for length scales of a kilometer and much slower for longer length scales. One then expects that horizontal density fluctuations on scales of a few kilometers disappear soon after they are created by forcing events like storms or wind bursts. This is consistent with the experimental evidence that typical thermohaline gradients on scales shorter than 10 km are compensated [3]. At scales of tens of kilometers nonlinear diffusion is not as efficient and it does not restore compensation between one forcing event and the next. The long term climatological $T-S$ relationship and the large scale density ratio of the ML are then the result of the competition between nonlinear diffusion, that dissipates horizontal density gradients, and thermohaline forcing, that continuously creates thermohaline anomalies.

The combined action of surface forcing and nonlinear diffusion on large scales in the ML is investigated with a model of the form given in (8) and (9). We restrict temperature and salinity to have spatial variations only in the meridional y-direction. A one dimensional model enables us to perform extensive Monte Carlo simulations and to obtain stable statistics of the thermohaline fields under the action of forcing. At the same time the one dimensional case capture the essential dynamics of thermohaline compensation; we verified that introducing a second dimension in simulations of the rundown problem does not change the dynamics that lead to the decay of density gradients. Only the process of thermohaline alignment cannot be captured in one dimension, but a characterization of the relative orientation of T and S gradients goes beyond the goal of this study. Here we limit our analysis to one dimensional statistics like the density ratio.

Numerical simulations of the nonlinear diffusion equations with forcing must be run for long times to achieve stable statistics. In order to save on CPU time, we limited our analysis of the equations in (8) and (9) to only one form of nonlinear diffusion. We chose the quadratic nonlinear diffusion that follows from a shear dispersion closure and set $f(|\nabla B|) = 1$. Only a few results depend on this particular choice and we will point them out. In one dimension the equations for T and S reduce to

$$T_t = \gamma(B_y^2 T_y)_y - \alpha(T - \theta(y)) + G(y,t). \tag{18}$$

$$S_t = \gamma(B_y^2 S_y)_y + F(y,t), \tag{19}$$

In the temperature equation (18), θ is the long time averaged atmospheric temperature determined by climatological data and $\alpha(T-\theta)$ represents the atmospheric feedback on the temperature of the ML: the larger $T-\theta$, the larger the heat flux from the atmospheric boundary layer into the ocean ML. $G(y,t)$ represents all other sources of heat such as daily and seasonal temperature variations. In the following numerical calculations $G(y,t)$ is set to zero under the assumption that the long term surface temperature is dominated by the climatological forcing rather than by the short term temperature fluctuations. The parameter

α sets the time scale needed for the ocean ML to adjust to the atmospheric temperature θ. When this time scale is small compared to the characteristic time scale of nonlinear diffusion, the equation for temperature reduces to

$$T = \theta(y) \tag{20}$$

The parameter α is determined by the time averaged heat flux from the atmosphere to the ocean and for a 100 m deep ML it is taken to be 10^{-7} s^{-1} [12]. For climatological gradients (6 °C over 1000 km) the nonlinear diffusion term is three orders of magnitude smaller than the relaxation term and (20) is a very good approximation of the equilibrated temperature field. Numerical simulations will show that this is indeed the case.

In the salinity equation (19), $F(y,t)$ represents the combined action of salinity fluxes across the air-sea interface (evaporation and precipitation) and across the base of the ML (entrainment of thermocline waters). The forcing on salinity $F(y,t)$ is modeled in the form of localized sources and sinks randomly distributed in space and time. Each forcing event create a salinity anomaly of the order of 0.01 psu in one day, equivalent to 3 cm of freshwater dumped in a 100 m deep ML or equivalently to an entrainment of 2 m of water with a salinity larger/smaller of 0.5 psu. We adjust the size and frequency of the forcing events so that we obtain the equivalent of a precipitation of 1 m per year, a value typical at midlatitudes in the North Pacific and in the North Atlantic [13], [14]. In order to conserve salinity the integral of the forcing on salinity must have zero average over long times,

$$\lim_{T\to\infty} \int_0^T \mathrm{d}t \int_0^L \mathrm{d}y F(y,t) \ = 0. \tag{21}$$

We impose this constraint by prescribing $F(y,t)$ as the sum of five positive and five negative Gaussians, all of the same amplitude, so that their sum is identically zero at all times. The positions of the Gaussians within the $L = 1000$ km of the domain is sampled from a uniform probability distribution and is changed every day. This ensures that the long time average forcing is zero at each point, even though several Gaussians can hit in the same place over a short period of time and produce strong local salinity and buoyancy gradients.

The key element of the problem set in (18) and (19) is that there is an asymmetry in the large scale forcing of temperature and salinity. Temperature is relaxed to some atmospheric climatological mean, while salinity is forced by random rainfall, evaporation and entrainment. The idea that asymmetries in the thermohaline forcing together with nonlinear parameterizations of eddy fluxes produce the observed large scale mean density ratio has been raised by Stommel [4]. Stommel tested this hypothesis with an idealized two-box model of the ML, but did not attempt any comparison with observations. Here we explore the process in the context of a continuous model of the ML and we quantify its effect for realistic oceanographic parameters.

4.1 Numerical algorithm

For the simulations we use dimensionless variables. Temperature and salinity gradients are measured in terms of of the climatological temperature gradient (6 °C over 1000 km), lengths

in terms of the domain length (1000 km) and the time in terms of the time it takes to mix tracers across the domain (3000 years).

The numerical calculations are performed by integrating the non dimensional equation for the temperature and salinity gradients, obtained by differentiating (18) and (19) in y,

$$(T_y)_t = \left(B_y^2 T_y\right)_{yy} - \alpha(T_y - \theta_y) - \mu(T_y)_{yyyy}. \quad (22)$$

$$(S_y)_t = \left(B_y^2 S_y\right)_{yy} + F_y - \mu(S_y)_{yyyy}, \quad (23)$$

The hyperviscosity is introduced to dissipate small scale gradients and to allow longer time stepping in the simulations. In this section we are interested in the effect of nonlinear diffusion on large scales and we do not need to resolve small scale structures. We use a grid spacing of 1 km and choose a value for μ that filters out all fluctuations with length scales shorter than 3 km. Global conservation of heat and salt is satisfied by requiring that $T_y = T_{yyy} = 0$ and $S_y = S_{yyy} = 0$ at both ends of the domain (i.e., no-flux boundary conditions). We solve the system in (22) and (23) on a discrete spatial grid with an explicit Euler forward scheme in time and a dealiased sine spectral code in space. The time step is set by the decorrelation time of the stochastic forcing acting on salinity, chosen to be one day.

4.2 The effect of stochastic forcing on salinity

The vision of the large scale $T - S$ relation in the ML is that the enormously variable forcing creates salinity anomalies that are eliminated by nonlinear diffusion. The combination of strong forcing on salinity and nonlinear eddy fluxes holds the average density ratio to a constant value. It is instructive to study the decay of a localized salinity anomaly to understand how the $T - S$ relationship is established.

Let us study the evolution of T and S after the forcing has created a large scale salinity anomaly. We prescribe a linear climatological gradient ($\theta_y = 1$) and we assume that the relaxation time scale is so fast (large α limit) that temperature is always in equilibrium ($T_y = 1$). In this limit the nonlinear diffusion equation for salinity reduces to,

$$S_t = \left[(S_y - 1)^2 S_y\right]_y - \mu(S_y)_{yyyy}, \quad (24)$$

We take the initial salinity profile to have the same width and shape of the Gaussian salinity anomalies created by F in (19). Figure 5 shows the profiles of S and S_y at time zero and at some later time. Salinity is diffused faster where the initial profile has a negative slope than where it has a positive slope. This asymmetry is easily explained if we consider that for a gradient of given magnitude $|S_y|$ the nonlinear diffusivity $(S_y - 1)^2$ is larger where S_y is negative than when S_y is positive. A look at the profiles of salinity gradients confirms that S_y diffuses at a slower rate when it has a value close to 1. As expected, in the absence of forcing, salinity decays to the only stable solution $S_y = 0$ (the solution $S_y = 1$ is only semistable), but regions where the salinity gradient is close to one decay slowly. We speculate that averaging the solution over many independent forcing events will reflect this asymmetry and produce a positive average salinity gradient $\langle S_y \rangle$; i.e., the presence of a climatological gradient $\theta_y = 1$ breaks the symmetry in the decay of the salinity gradients and determines a finite mean density ratio $R = 1/\langle S_y \rangle$.

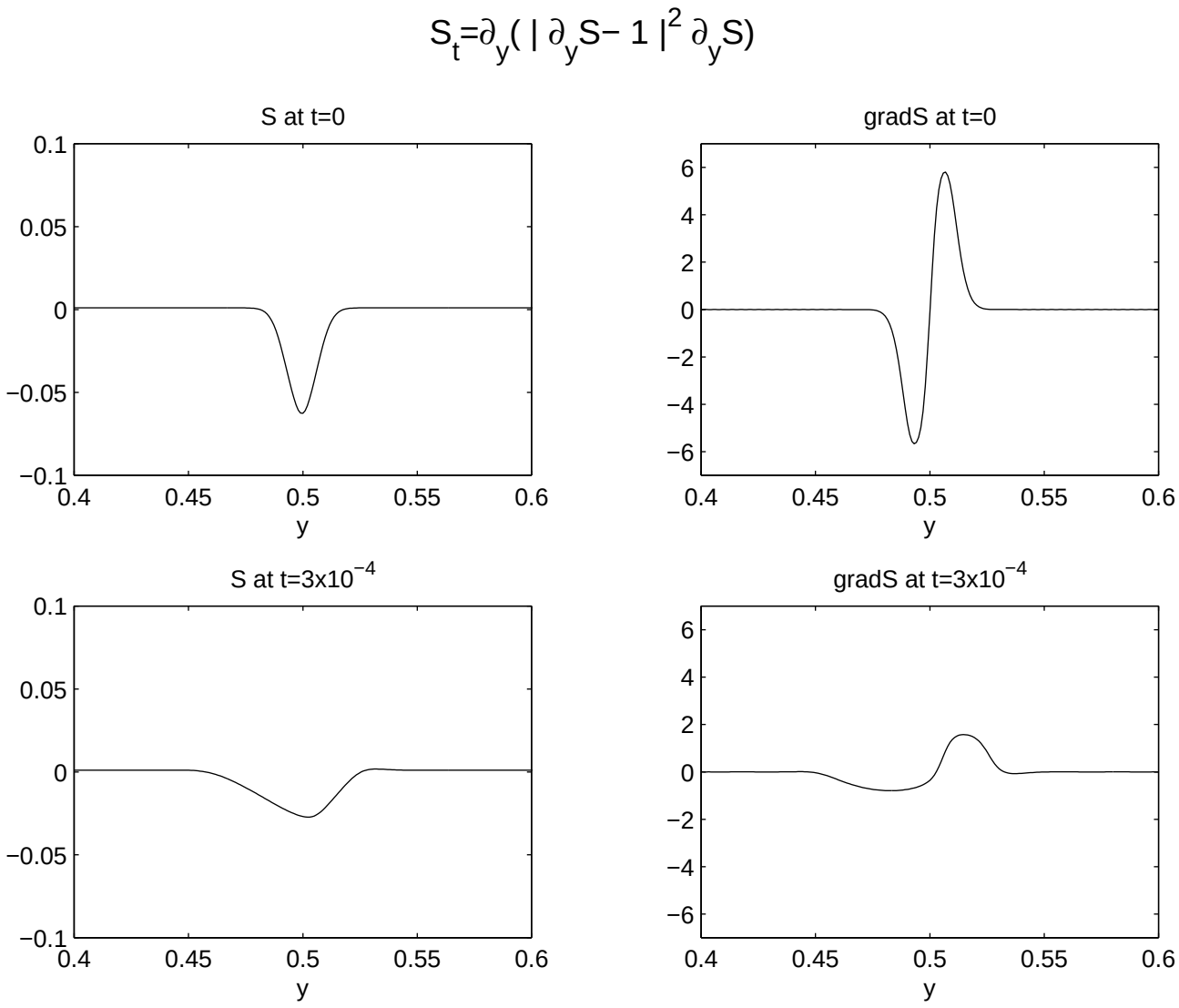

Figure 5: Evolution of a Gaussian salinity anomaly subject to the nonlinear diffusion equation in (24). The upper panels show the initial salinity and salinity gradient and the lower panels the same variables at a later time. Only the central part of the integration domain is shown.

Some general properties of the evolution of the salinity gradient are better revealed by writing equation (23) in variational form,

$$(S_y)_t = \partial_y^2 \left[\frac{\delta \Phi}{\delta S_y} \right] + F_y, \tag{25}$$

where $\Phi(S_y)$ is the functional

$$\Phi(S_y) \equiv \int_0^1 \left[H(S_y, y) + \frac{1}{2}\mu (S_{yy})^2 \right] \mathrm{d}y \tag{26}$$

and $H(S_y, y)$ is the function

$$H(S_y, y) = \frac{1}{4} S_y^4 - \frac{2}{3}\theta_y S_y^3 + \frac{1}{2}\theta_y^2 S_y^2. \tag{27}$$

In (25) we introduced the variational derivative of the functional $\Phi(S_y)$,

$$\frac{\delta \Phi}{\delta S_y} = H_{S_y} - \mu S_{yy}. \tag{28}$$

In the absence of forcing, the form (25) can be used to show that the system has only one stable equilibrium which minimizes the functional $\Phi(S_y)$, i.e., $S_y = 0$ (figure 27). Furthermore the shape of the potential is such that the decay towards equilibrium is slower around the saddle line $S_y = \theta_y$. We then expect that, even though the random forcing creates positive and negative S_y anomalies with the same probability, salinity gradients with values close to zero and θ_y are more persistent and the long time averaged salinity gradient at each point settles to some value between zero and θ_y.

4.3 Numerical simulations

We begin our numerical experiments of the system in (22) and (23) by relaxing temperature towards a linear climatological gradient; i.e. we set $\theta_y = 1$ in (22). The initial temperature and salinity gradients are chosen to be zero. The model is run continuously for 3200 years.

During the first stages of the simulation the thermohaline fields evolve from the initial conditions towards a statistically steady state. Temperature relaxes to the climatological mean in a few years. After that fluctuations from the equilibrium solution $T(y,t) = \theta(y)$ are negligible. The spin up time for salinity is approximately 200 years. In the following all statistics are computed discarding this initial spin up time.

Figure 7 shows the mean thermohaline fields averaged over 3000 years. In the upper left panel, T and S profiles are plotted as a function of latitude. Salinity develops a large scale structure, even though the random forcing is uniformly distributed in the domain. The long time average profile of salinity is, to a good approximation, $S = (2/3)y$. The analog of the oceanographic mean horizontal density ratio for this model is $R = \overline{T_y}/\overline{S_y} = 3/2$, where the overbars denote the temporal averaging. A mean density ratio of 1.5 on a scale of 1000 km, the size of our domain, is consistent with the observational results of Stommel and Chen [4], [5]. Notice though that our averages are carried over 3000 years, while both Stommel and

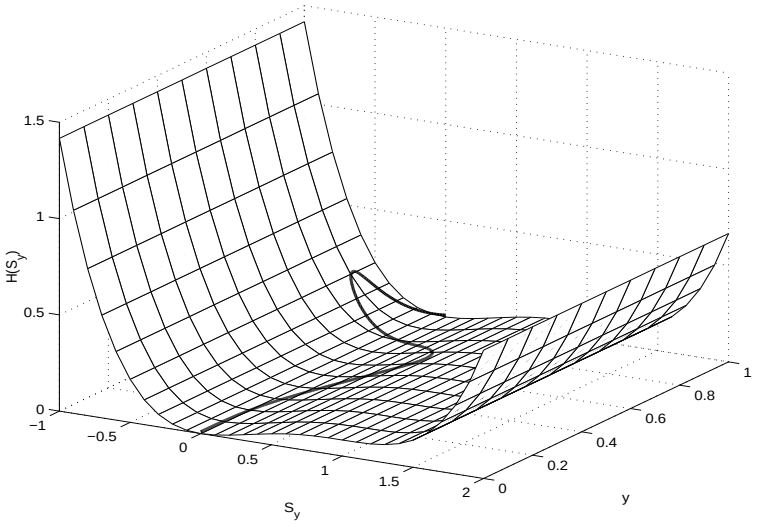

Figure 6: The function $H(S_y)$ in the case of a linear climatological temperature gradient, i.e., $\theta_y = 1$. The dark line is a possible S_y profile.

Chen used climatologies averaged over less than 20 years. We return to this point at the end of the section.

Simple arguments based on a Reynold's decomposition of the thermohaline fields are now used to interpret the density ratio of 3/2 obtained in the numerical simulations. Let us decompose S and T as the sum of a temporal mean plus fluctuations about that mean; i.e., $S = \overline{S} + S'$ and $T = \overline{T} + T'$. Numerical experiments show that we can safely neglect T' in the Reynold's decomposition of T and write $T = \overline{T} = \theta$. Taking the time average of the nonlinear diffusion equation for salinity then gives,

$$\overline{S_t} = \left(\overline{S_y'^3} + \overline{S_y'^2}(3\overline{S_y} - 2\theta_y) + \overline{S_y}(\overline{S_y} - \theta_y)^2\right)_y + \overline{F}. \tag{29}$$

Both $\overline{F}$ and $\overline{S_t}$ vanish if the average is carried over a long enough time. The sum of the first three terms in the RHS of (29) must then vanish as well. Notice that this sum cannot be a constant different from zero, because of the no-flux boundary conditions. Furthermore, the third term, $\overline{S_y}(\overline{S_y} - \theta_y)^2$, is likely to be smaller than the first two, because the typical amplitude of the fluctuations created by the forcing is larger than the mean gradients; numerical results show that this is indeed the case (last panel of figure 7). Therefore the leading order balance involves only the first two terms. Setting to zero $\overline{S_y'^3} + \overline{S_y'^2}(3\overline{S_y} - 2\theta_y)$ gives an estimate of the mean salinity gradient,

$$\overline{S_y} = \frac{2}{3} - \frac{\overline{S_y'^3}}{\overline{S_y'^2}}. \tag{30}$$

The numerical simulations show that $\overline{S_y'^2}$ settles to a constant profile different from zero, while $\overline{S_y'^3}$ keeps decreasing throughout the domain. This explains why $\overline{S_y}$ asymptotes 2/3 when

averaged over long times. Finally we should remark that we did not include the hyperviscosity term in this analysis, because its contribution in the long term balance is maintained small by choosing an appropriate value for μ.

The Reynold's decomposition analysis of the equations in (22) and (23) shows that a large scale mean salinity gradient is required if all nonlinear fluxes are to balance when averaged over long times. This balance depends on the particular form of nonlinear diffusion chosen. That is nonlinear closures different from $f(|\nabla B|) = 1$ in (8) and (9) would still produce a large scale salinity gradient, but its dependence on θ_y would not be that given in (30). Stommel came to the same conclusion for his two box model [4]. He obtained that, for a diffusivity between the two boxes of the form $|B_y|^n$, the salinity gradient becomes linearly proportional to the climatological temperature gradient and the mean density ratio approaches $(n+1)/n$. We verified that Stommel argument applies also in the continuous limit for the diffusivity B_y^2.

So far we showed thermohaline profiles averaged over 3000 years. Averaging over shorter times gives results that are not in statistical equilibrium. Results averaged over two different subintervals of 30 years from the same simulation shown in figure 7 give a density ratio close to 3/2 in one case (figure 8) and 1 in the second case (figure 9). The differences arise because over 30 years the leading order balance in (29) involves both $\overline{S_t}$ and $\overline{F}$. It is necessary to average over longer times to include a number of forcing events large enough to obtain stationary statistics. Over a 3000 year time span, each point on the grid is hit on average by 10^6 forcing events, while over a 30 year time span this number is one hundred times smaller and as a consequence the average of the forcing is 10 times larger: it is the number of independent forcing events that sets the time required to have stable statistics. In this sense our results are consistent with observations, because in their analysis Stommel and Chen compute averages over a wide range of longitudes in space so that they include many realizations of forcing events per unit time.

5 Discussion

The main result of this project is that nonlinear diffusive parameterizations of the ML, which use buoyancy as the driving field, can explain the different values of density ratio observed in oceanographic measurements. At scales shorter than 10 km the nonlinear fluxes are so strong that a horizontal density ratio of 1 is restored in a few days whenever a forcing event creates an anomaly in T and S. At larger scales the correlations between temperature and salinity emerge as a balance between nonlinear diffusion and thermohaline forcing. The large scale forcing on temperature is modeled as a relaxation of temperature towards a climatological mean profile to account for the atmospheric feedbacks on thermal anomalies. There is no reason to include an analogous term in the equation for salinity and the forcing on salinity is purely stochastic. The difference in the forcings breaks the symmetry between T and S. The large scale temperature gradient relaxes in a few years towards the climatological mean, while salinity develops a large scale gradient that on average is proportional to that of temperature even though the forcing on salinity is uniformly distributed over the domain. The ratio of the large scale mean gradients of T and S is close to 3/2 for the specific nonlinear diffusion parameterization used in the simulations. This value is consistent with observations.

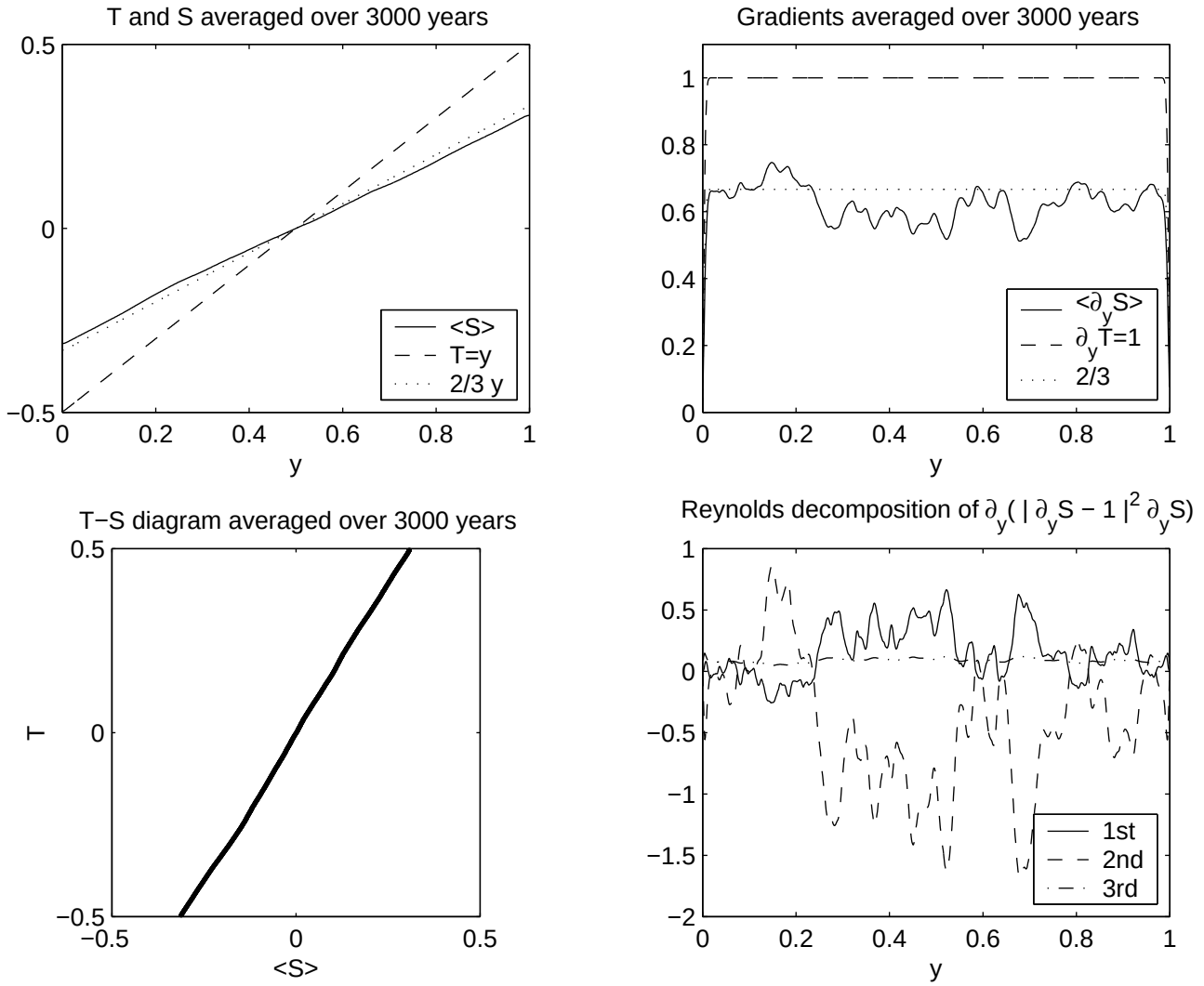

Figure 7: Results of a numerical simulation of the system in (22) and (23) with $\theta = y$ and 1000 grid points. The upper panels show the T, S, T_y and S_y profiles as a function of latitude y, averaged over 3000 years. The average salinity compensates 2/3 of the climatological temperature gradient. The lower left panel is the $T - S$ diagram of the averaged T and S profiles. The lower left panel is a plot of the first three terms in the RHS of (30); $\overline{S_y'^3}$ is the continuous line, $\overline{S_y'^2}(3\overline{S_y} - 2\theta_y)$ is the dashed line and $\overline{S_y}(\overline{S_y} - \theta_y)^2$ is the dashdotted line.

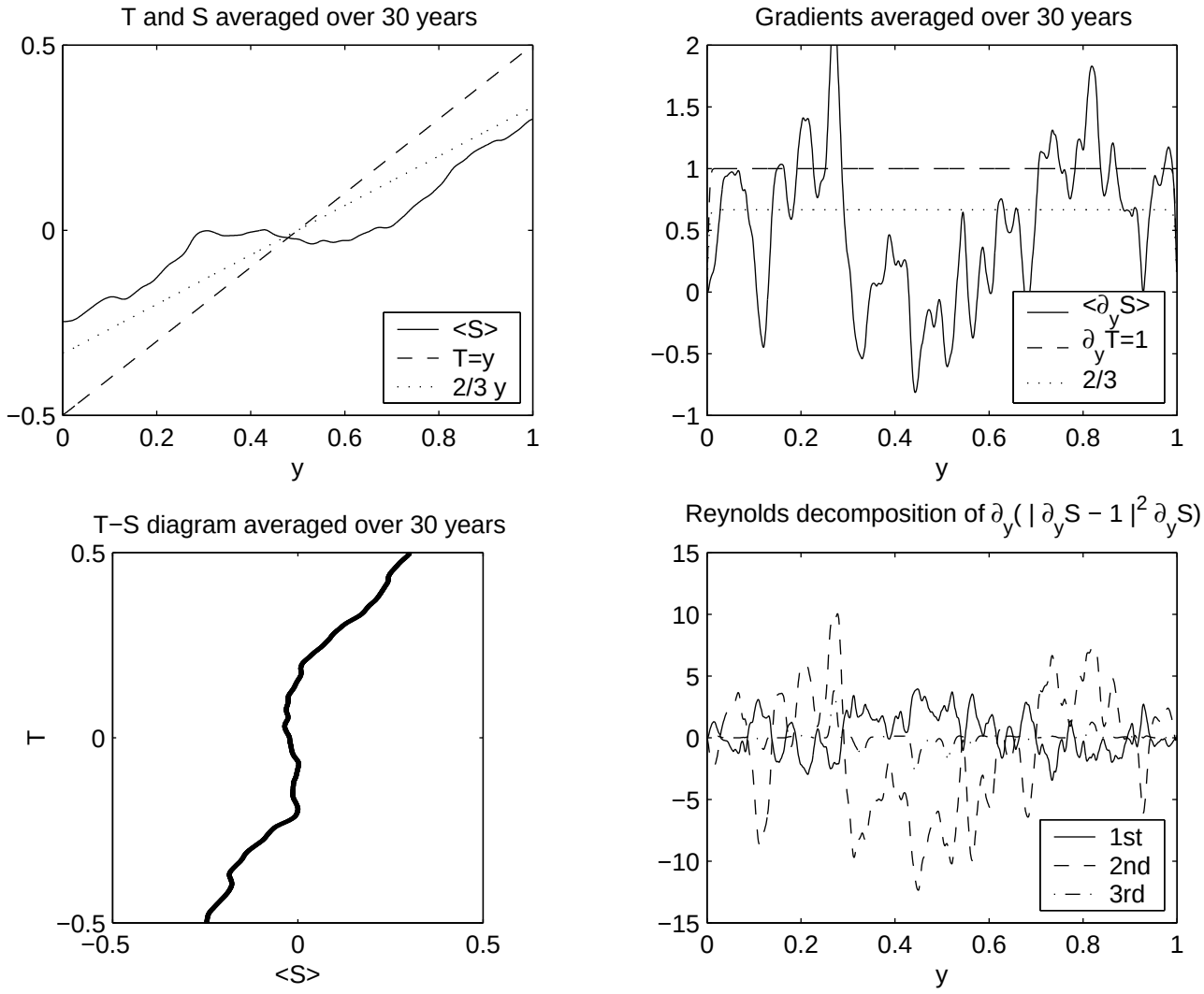

Figure 8: Results from the same simulation shown in figure 7 averaged over a subinterval of 30 years.

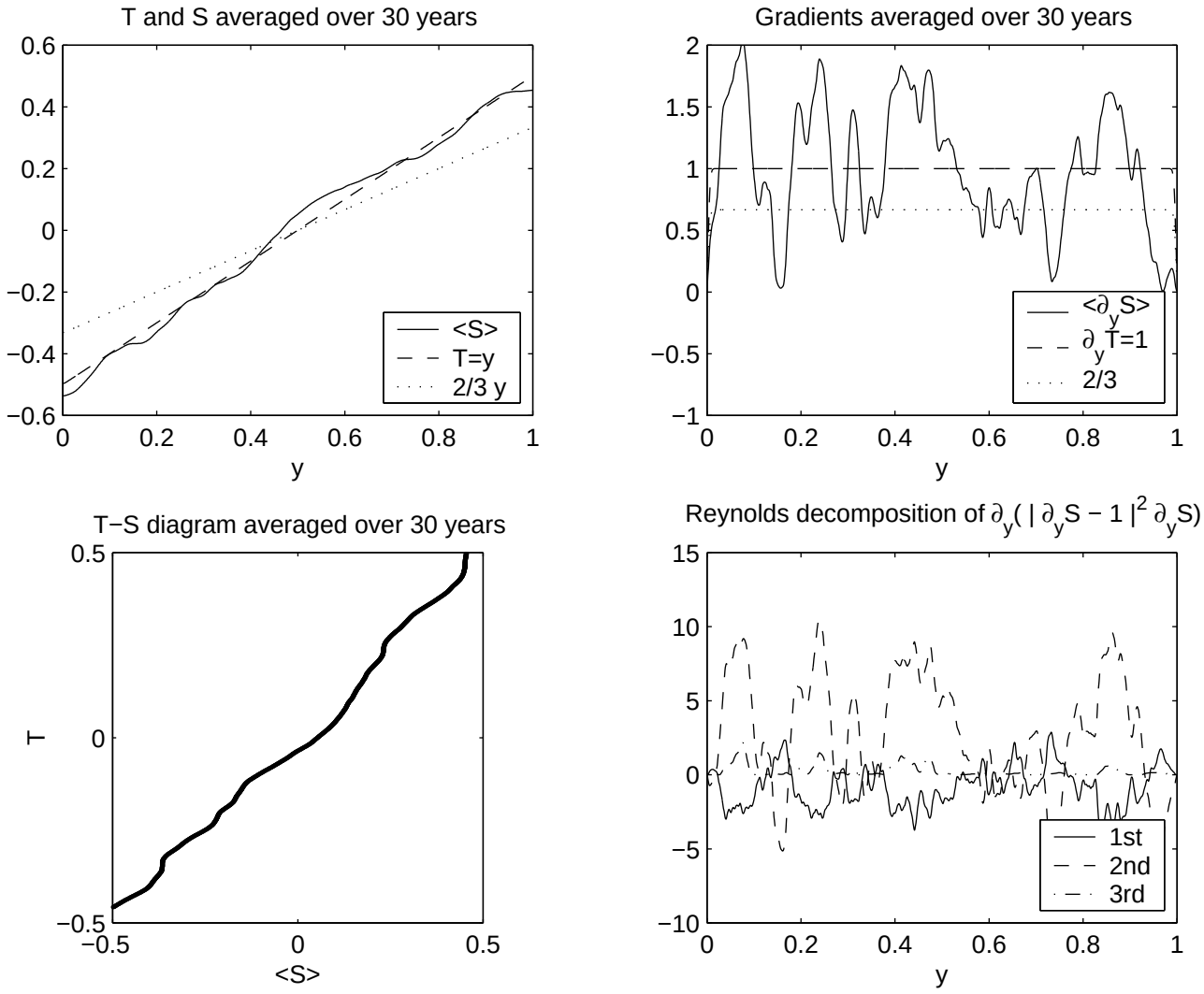

Figure 9: Results from the same simulation shown in figure 7 averaged over a subinterval of 30 years.

In order to show both a density ratio of 1 at small scales and a density ratio of 1.5 at large scales, we are running numerical simulations of the equations in (18) and (19) with stochastic noise on temperature and salinity; that is $G(y,t)$ and $F(y,t)$ have a white spectrum in space and time. Preliminary results show that compensation develops over a few grid points and produce a small scale density ratio of 1, while at large scales salinity compensates only part of the temperature gradient and the density ratio settles to 1.5.

In our model the instantaneous distribution of buoyancy gradients at large scale is determined by the most recent forcing events. On the other hand observations in the ML of all oceans show that buoyancy fronts tend to concentrate in regions of Eckman convergence. The analysis of nonlinear diffusion models with a large scale advection that has regions of convergence is a direction for future research. The hypothesis is that the stochastic forcing creates buoyancy anomalies uniformly throughout the domain and the advective field collects them towards regions of convergence. The result is that the average density ratio is still 3/2, but it is all due to a few localized gradients.

Finally, it would be instructive to implement nonlinear diffusive parameterizations of the thermohaline eddy fluxes in large scale ocean models. It is well known that ocean models tend to produce unrealistic distributions of salinity in the ML, because there is no feedback mechanism that maintains large scale salinity anomalies within reasonable bounds. Typically the cure is to introduce some ad hoc relaxation to observations. Nonlinear diffusive parameterizations obtain the same result by introducing an indirect feedback through the climatological temperature gradient. Furthermore the parameterizations we have discussed in this project are the results of closures based on sound physical arguments and are not dictated by numerical necessity. An obvious goal is to test the different nonlinear parameterizations against the observed density ratio to infer which are more appropriate.

Acknowledgments

I am grateful to all the staff and fellows of the GFD Summer Program for a most enjoyable and instructive summer. I am especially thankful to Joe Keller and Eric Chassignet for many enlightening conversations, Paola Cessi for her invaluable help with the numerics and Bill Young for numerous suggestions in some critical moments. Thanks to Ed Spiegel, George Veronis, Jean-Luc Thiffeault, Francesco Paparella and our director Neil Balmforth for all their help and encouragement.

References

[1] G. I. Roden, "The vertical thermohaline structure in the argentine basin," J. Geophys. Res. **94**, 877 (1989).

[2] D. L. Rudnick and J. R. Luyten, "Intensive survey of the azores front. 1. tracers and dynamics," J. Phys. Ocean. **101**, 923 (1996).

[3] D. L. Rudnick and R. Ferrari, "Compensation of horizontal temperature and salinity gradients in the ocean mixed layer," Science **283**, 526 (1999).

[4] H. M. Stommel, "A conjectural mechanism for determining the thermohaline structure of the oceanic mixed layer," J. Phys. Ocean. **23**, 142 (1993).

[5] L. G. Chen, "Mixed layer density ratio from the levitus data," J. Phys. Ocean. **25**, 691 (1995).

[6] H. M. Stommel, "Theromhaline convection with two stable regimes of flow," Tellus **13**, 224 (1961).

[7] H. M. Stommel and W. R. Young, "The average t-s relation of a stochastically forced box model," J. Phys. Ocean. **23**, 151 (1993).

[8] R. Ferrari and W. R. Young, "On the development of theromhaline correlations as a result of nonlinear diffusive parameterizations," J. Mar. Res. **55**, 1069 (1997).

[9] J. A. Green, "Transfer properties of the large-scale eddies and the general circulation of the atmosphere," Quart. J. Roy. Meteorol. Soc. **96**, 157 (1970).

[10] P. H. Stone, "A simplified radiative-dynamical model for the static stability of rotating atmosphere," J. Atmos. Sci. **29**, 405 (1972).

[11] V. Pavan and I. M. Held, "The diffusive approximation for eddy fluxes in baroclinically unstable jets," J. Atmos. Sci. **53**, 1262 (1996).

[12] R. L. Haney, "Surface thermal boundary conditions for ocean circulation models," J. Phys. Ocean. **1**, 241 (1971).

[13] R. K. Reed and W. P. Elliott, "New precipitation maps for the north atlantic and north pacific oceans," J. Geophys. Res. **84**, 7839 (1979).

[14] P. S. B. R. W. Schmitt and C. E. Dorman, "Evaporation minus precipitation and density fluxes for the north atlantic," J. Phys. Ocean. **19**, 1208 (1989).